

Rapid Velocity-Encoded Cine Imaging with Turbo-BRISK

Mark Doyle, Eduardo Kortright, Andreas S. Anayiotos,
Abdelaziz M. Elmahdi, Edward G. Walsh, Anthon R. Fuisz,
and Gerald M. Pohost

*Department of Medicine, Division of Cardiovascular Disease, University of
Alabama at Birmingham, Birmingham, Alabama*

ABSTRACT

Velocity-encoded cine (VEC) imaging is potentially an important clinical diagnostic technique for cardiovascular diseases. Advances in gradient technology combined with segmentation approaches have made possible breathhold VEC imaging, allowing data to be obtained free of respiratory artifacts. However, when using conventional segmentation approaches, spatial and temporal resolutions are typically compromised to accommodate short breathhold times. Here we apply a sparse sampling technique, turbo-BRISK (i.e., segmented block regional interpolation scheme for k-space) to VEC imaging, allowing increased spatial and temporal resolution to be obtained in a short breathhold period. BRISK is a sparse sampling technique with interpolation used to generate unsampled data. BRISK was implemented to reduce the scan time by 70% compared with a conventional scan. Further, turbo-BRISK scans, using segmentation factors up to 5, reduce the scan time by up to 94%. Phantom and in vivo results are presented that demonstrate the accuracy of turbo-BRISK VEC imaging. In vitro validation is performed using conventional magnetic resonance VEC. Pulsatile centerline flow velocity measurements obtained with turbo-BRISK acquisitions were correlated with conventional magnetic resonance imaging measurements and achieved r values of 0.99 ± 0.004 (mean \pm SD) with stroke volumes agreeing to within 4%. A potential limitation of BRISK is reduced accuracy for rapidly varying velocity profiles. We present low- and high-resolution data sets to illustrate the resolution dependence of this phenomenon and demonstrate that at conventional resolutions, turbo-BRISK can accurately represent rapid velocity changes. In vivo results indicate that centerline velocity waveforms in the descending aorta correlate well with conventional measurements with an average r value of 0.98 ± 0.01 .

KEY WORDS: *Fast imaging; Flow; k-space; VEC; Vascular.*

Received May 25, 1998; Accepted December 4, 1998

INTRODUCTION

Phase-based velocity-encoded cine (VEC) imaging has been shown by many investigators to provide accurate quantitative flow information with pixel resolution and to have clinical application (1–11). However, a feature of VEC imaging is that data are resolved over the heart cycle, substantially prolonging the acquisition time. Additionally, blood-flow patterns in cardiac chambers and great vessels are generally complex and require measuring velocity in three dimensions, which further prolongs the acquisition time (12). Thus, phase velocity mapping applied to the cardiovascular system, although feasible, is time consuming and requires the development of rapid acquisition strategies to achieve clinical utility.

Because phase velocity mapping requires the combination of two data sets (either velocity compensated and velocity encoded or positive and negative velocity encoded), it is potentially sensitive to respiratory artifacts. Data acquired under breathhold conditions typically contain fewer artifacts compared with non-breathhold data sets but at the expense of increased motion blur and reduced spatial resolution due to increased acquisition times within each cardiac cycle (13–17). Thus, in many applications, compromises in the segmentation factor, spatial resolution, and breathhold duration are made (18).

To date, reductions in scan time have accompanied advances in gradient technology. However, state-of-the-art gradient sets (with slew rates in the range of 100 to 150 mT/m/msec) are currently limited not by gradient technology but by the physiologically acceptable limit of dB/dt (to avoid stimulating muscular spasms). Higher gradient strengths are also associated with higher receiver bandwidths, leading to lower signal-to-noise ratios. These restrictions present substantial obstacles to further reduction of acquisition time due purely to advances in gradient hardware. Although future improvements in gradient technology might one day overcome these obstacles, at present other means of reducing scan duration are required to promote the clinical utility of VEC imaging and allow its extension to further applications (19).

We and other investigators have shown that for dynamic cardiovascular imaging, variable sampling rate strategies can be applied to limit motion artifacts and reduce scan times while maintaining spatial resolution (20,21). For the specific case of VEC cardiac imaging, Liao et al. (22) demonstrated that most dynamic information is concentrated toward the center of k-space. Recently, we introduced BRISK (block regional interpola-

tion scheme for k-space), a rapid scanning strategy that we applied to reduce the acquisition time for gradient echo cardiac cine acquisitions (21). BRISK is a sparse sampling strategy that acquires data over the cardiac cycle at varying rates (a high sampling rate is applied to the central lines of k-space and progressively slower rates are applied to outer lines). In the BRISK strategy, data that are not directly acquired are retrospectively generated by Fourier interpolation over the full cardiac cycle. BRISK acquires a typical cardiac cine image set in 30% of the conventional scan time, a time reduction comparable with using a segmentation factor of 3. The first application of the BRISK approach to VEC imaging was implemented by Jhooti et al. (23). Further reductions in acquisition time are possible by combining BRISK with the segmentation strategy to obtain the turbo-BRISK scan (i.e., a segmented version of BRISK) (24). Standard phase velocity mapping has been verified at multiple sites (including ours) to accurately (typically within 7%) quantify steady-state flow in phantoms (25,26). Additionally, the accuracy of VEC imaging applied to pulsatile flow imaging has been established for conventional gradient echo, spiral, and segmented gradient echo imaging methods to be within 7% (16,26–28). Here we apply BRISK and turbo-BRISK VEC imaging to pulsatile flow and compare it with conventional magnetic resonance imaging (MRI) and electromagnetic flow (EMF) probe measurements *in vitro*. Additionally, *in vivo* breathhold turbo-BRISK VEC images are compared with conventional MR images acquired over 4 min.

METHODS

Conventional, BRISK, and turbo-BRISK VEC imaging was performed in a pulsatile flow phantom. Validation was performed using EMF measurements. *In vivo* acquisitions using conventional MRI and turbo-BRISK were performed in five normal volunteers imaged at the level of the descending aorta. Unless otherwise stated, results are quoted as mean \pm SD.

In Vitro Measurements

The conventional gradient echo-based VEC imaging sequence available on our scanner (Philips ACS, 1.5 T, Best, The Netherlands) was modified to accommodate BRISK and turbo-BRISK acquisitions (21,24). The scanner is equipped with gradients with a maximum strength of 10 mT/m and a maximum slew rate of 10 mT/m/msec. In our implementation of VEC, velocity-compensated

and velocity-encoded data sets were acquired in an interleaved manner (i.e., the velocity-compensated data were acquired in one heart cycle and the corresponding velocity-encoded data were acquired in the next). In the presence of motion and flow variations, this approach allows close coupling of acquisition conditions between velocity-compensated and velocity-encoded k-space lines. A Harvard flow pump (Harvard Apparatus 1421 pulsatile flow pump, South Natick, MA) was used to generate pulsatile flow representative of human aortic flow: Stroke volume was set at 100 ml, systolic/diastolic ratio was 30%, and the pump rate was 60 beats per minute. The maximum centerline velocity was approximately 100 cm/sec, and the maximum Reynolds number was calculated to be 22,000, indicating turbulent conditions at peak flow. Synchronization of the spectrometer with the pump cycle was accomplished by the pump's triggering circuitry. The flow test section consisted of a rigid circular cross-section Plexiglas tube of inner diameter 18.9 mm and length 15 cm, connected to the pump via flexible polyvinyl chloride tubing. The fluid used was a copper sulfate water solution. Phantom scans were performed at large (300 mm) and small (190 mm) fields of view (FOV). Parameters used were flow sensitivity ± 150 cm/sec, matrix 256×256 , slice thickness 8 mm, and full echo acquisition. For the 300-mm FOV acquisitions, TR/TE/flip were 16/9.2/40°, and for the 190 FOV acquisitions, TR/TE/flip were 21/12.5/40°. All data were acquired using a body coil. Conventional and BRISK scans were performed in addition to turbo-BRISK acquisitions with turbo factors ranging from 2 to 5. Data were acquired over the complete pump cycle starting after a delay of 8 msec from the trigger point. Details of scan parameters for the phantom are given in Table 1.

Stroke volume was measured using a blood flow probe

(model EP675P1, Carolina Medical Inc., King, NC) along with a square-wave electromagnetic flow meter (model FM 501D, Carolina Medical). The EMF probe was incorporated upstream from the test section, and data were acquired and recorded using a computer with a National Instruments (Austin, TX) AT-MIO-16X data acquisition board and the virtual instrument software package LabVIEW.

In Vitro Data Analysis

For the BRISK and turbo-BRISK acquisitions, sparse k-space data were exported from the scanner's database for off-line processing on a SPARCstation 20 computer where temporal interpolation was performed to generate a complete k-space data set for each time frame. Modulus and phase images were generated on the SPARCstation using programs written in the Matlab (The Mathworks, Natick, MA) environment. All image analysis was performed in this environment, including production of velocity images by comparison of phase maps. At maximum flow rate conditions, velocity profiles and average velocities corresponding to the flow section center and four circumferential regions (at 3, 6, 9, and 12 o'clock positions) were plotted for each scan series. Calculations of vessel area, stroke volume, and maximum and minimum centerline velocities were made based on vessel boundaries found by means of threshold masks. These masks were derived from the mean of the modulus images for all phases, and the threshold was adjusted for each data set to approximately 13–14% of the maximum modulus image intensity for the low-resolution phantom and 33–35% for the high-resolution phantom. To allow comparison of data sets, data were standardized by interpolating to 128 time points. Fourier and regression analy-

Table 1
Parameters for Conventional, BRISK, and Turbo-BRISK VEC Acquisitions

	Conv	B1	B2	B3	B4	B5
Acq time (min:sec)	8:47	2:24	1:18	0:51	0:38	0:30
HPI (msec)	16/21	16/21	32/42	48/63	64/84	80/105
No. HPs	60/46	60/46	30/23	20/15	15/11	12/9

In fields with dual occupancy, the first number refers to the high FOV (300 mm) acquisition and the second number to the low FOV (190 mm) acquisition. Acquisition parameters are for a matrix of 256×256 and data are assumed to be acquired for approximately 95% of the cardiac cycle.

Acq time, total acquisition time assuming a heart rate of 60 bpm; HPI, the heart phase interval; No. HPs, number of heart phases acquired over the cardiac cycle; Conv, conventional scan; B1–B5, BRISK through turbo-BRISK 5 scans.

sis was conducted on the velocity waveform integrated over the vessel area. The number of Fourier coefficients with squared magnitude (i.e., energy) greater than 1% of that of the zeroth coefficient was determined. Correlation analysis was performed for the centerline velocity, comparing the conventional with BRISK data.

In Vivo Acquisitions

In five normal volunteers, turbo-BRISK breathhold scans were performed with matrix 256×128 , FOV 300 mm (in-plane resolution of 1.2×2.3 mm), turbo factor of either 3 or 4 (dependent on heart rate), scan time 20 sec, velocity sensitivity ± 150 cm/sec, TR/TE/flip 14/7/20°, and 75% partial echo. Partial echo acquisitions were used to reduce the heart phase interval for any given turbo factor. For each volunteer a conventional (non-breathhold) scan was also performed at 40 to 60 cardiac phases, depending on heart rate, with scan times ranging from 3 to 4 min. For all cases, a thoracic section of the descending aorta was imaged at a position approximately 10 cm distal to the aortic arch and flow data were extracted in a manner similar to the phantom analysis.

In Vivo Data Analysis

For the turbo-BRISK scans, k-space assemblage was performed off-line as with the *in vitro* data, and velocity map generation was performed using the scanner's standard image processing software. For each VEC image series, the frame corresponding to peak flow was determined, and using Matlab software, a mask was generated from the modulus image to define the extent of the vessel. The mask required manual editing to remove noise points. Using this mask, the average peak velocity, vessel area, and stroke volume were calculated. For the conventional and turbo-BRISK scans, velocity profiles resolved over the cardia cycle were plotted for two regions, one positioned over the center of the descending aorta and another positioned over static tissue. The turbo-BRISK and conventional images were Fourier interpolated to 128 time frames to allow direct comparison of waveforms, and Fourier, regression, and correlation analyses were performed for the *in vitro* data.

RESULTS AND DISCUSSION

In Vitro Results

The centerline velocity curves averaged over nine pixels for the 300-mm and 190-mm FOV data sets are com-

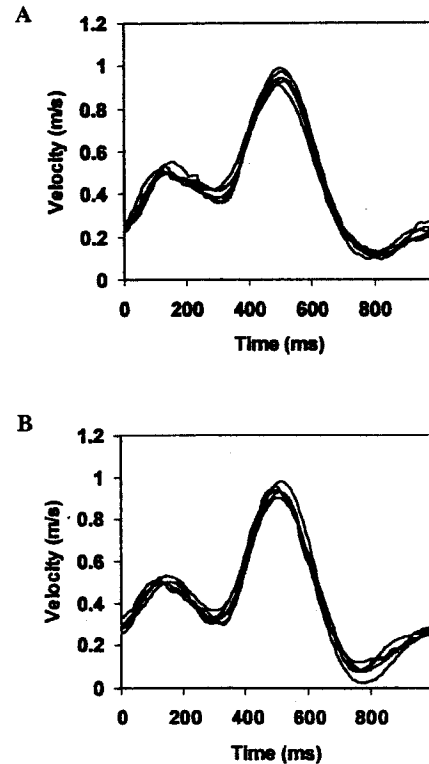


Figure 1. Centerline velocities resolved over time are plotted for (A) the low-resolution series and (B) the high-resolution series.

pared in Fig. 1. In the plots, the time origins of the turbo-BRISK data have been cyclically adjusted to synchronize with the conventional scan (12). Excellent correlation r values (0.99 ± 0.004) were obtained for centerline curves comparing conventional MRI with the BRISK series, with no trend associated with increasing turbo-BRISK factor. Flow parameters and regression results comparing turbo-BRISK with the conventional data are shown in Table 2 for the low-resolution data sets and in Table 3 for the high-resolution data sets. MRI estimates of vessel area were determined from threshold masks obtained individually for each data set and were in excellent agreement within each of the high- and low-resolution scan series and between the two series. The calculated stroke volumes were similarly in close agreement within each series and close to the 100 ml measured by the EMF probe. The slopes of the regression analysis were very close to unity (low resolution 1.0 ± 0.05 , high resolution 0.99 ± 0.05) and the intercept was very close to zero (low resolution 0.02 ± 0.02 , high resolution $0.06 \pm$

Table 2
Results Summary for the Low-Resolution In Vitro Study

	Stroke Volume (ml)	Area (mm ²)	Peak/Trough (cm/sec)	<i>r</i>	Slope	Intercept	SE
Conv	100	292	95/10	NA	NA	NA	NA
B1	102	297	97/10	0.99	1.06	-0.03	0.03
B2	100	297	94/12	1.00	1.02	0.00	0.02
B3	102	297	92/11	0.99	0.99	0.01	0.03
B4	102	298	98/13	0.99	1.04	0.01	0.03
B5	100	296	91/13	0.99	0.94	0.03	0.03

Scan series designations are the same as in Table 1. The peak/trough column represents the maximum and minimum velocity values for the central flow regions. The stroke volume calculated from the EMF measurements was 100 ml, and the theoretic vessel cross-sectional area was 280 mm². Correlation and regression analysis was performed against the conventional data. NA, not applicable.

0.03), indicating excellent agreement between conventional and turbo-BRISK data sets.

Flat velocity profiles that vary over time can present a severe challenge for the BRISK strategy. To investigate this, velocity profiles through the vessel center aligned along read and phase-encoding directions were plotted at peak flow. These profiles are shown in Fig. 2 for the low- and high-resolution series. As expected, the turbo-BRISK profiles aligned with the read direction better represent the relatively high-velocity gradients at the vessel boundaries compared with profiles aligned along the phase-encoding direction. This disparity is less pronounced in the high-resolution series, where it can be seen that profiles aligned with both the read and phase-

encoding directions retain sharp profiles for low-order turbo-BRISK acquisitions.

A more detailed investigation of the velocity response for BRISK and turbo-BRISK scans was performed by plotting regional velocities at peak flow against the scan series for five regions as shown in Fig 3. Regions close to the vessel wall were positioned over the area of maximum deviation from the 100% scan. For both the low- and high-resolution series, peak velocity in the central region is accurately represented for the full range of turbo-BRISK scans. Additionally, in the low resolution series, circumferential region pairs aligned along the read-encoding direction are accurately represented, whereas region pairs along the phase-encoding direction

Table 3
Results Summary for the High-Resolution In Vitro Study

	Stroke Volume (ml)	Area (mm ²)	Peak/Trough (cm/sec)	<i>r</i>	Slope	Intercept	SE
Conv	96	277	94/8	NA	NA	NA	NA
B1	96	274	96/7	1.00	0.99	0.01	0.02
B2	96	275	93/8	0.99	1.00	0.01	0.04
B3	95	275	90/12	0.99	1.06	-0.03	0.03
B4	95	275	94/2	0.99	0.93	0.04	0.03
B5	96	276	98/8	0.99	0.96	0.00	0.04

Scan series designations are the same as in Table 1. The peak/trough column represents the maximum and minimum velocity values recorded for the central flow regions. The stroke volume calculated from the EMF measurements was 100 ml, and the theoretic vessel cross-sectional area was 280 mm². Correlation and regression analysis was performed against the conventional data. NA, not applicable.

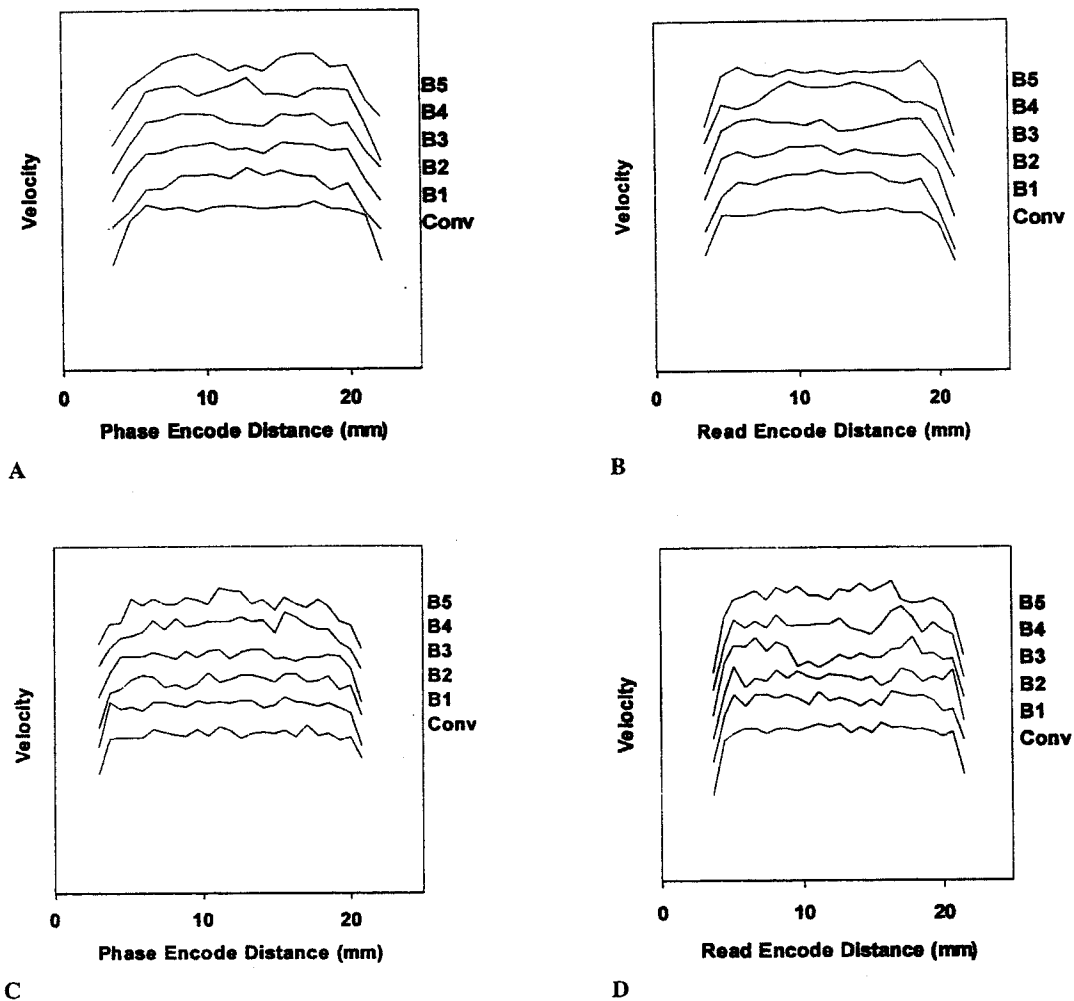


Figure 2. Velocity profiles for the low-resolution scan, aligned along (A) the phase-encoding direction and (B) the read direction, with corresponding profiles for the high-resolution scans shown in C and D. To allow details to be visualized, the plots have been offset by uniform progressive amounts, because all profiles essentially overlaid one another. Conv, conventional.

exhibit a uniform decrease in velocity by an average of 9% for the BRISK series compared with the conventional scan. The high-resolution series in Fig. 3, C and D shows that for region pairs along both major directions, velocities are accurately represented for low-order turbo-BRISK factors but accuracy diminishes with increasing turbo-BRISK factor. This reduction in measured peak velocity for pulsatile flow waveforms has previously been noted as a limitation of segmentation methods (16). Fourier analysis of the integrated velocity over the vessel cross-section for the conventional low- and high-resolution data sets revealed that energy fell to below 1% of

that of the zeroth coefficient after 3 coefficients (for a 128 time-point function).

The interaction of spatial and temporal resolution effects in rapid imaging of pulsatile flow through a vessel with BRISK and turbo-BRISK is complex. Higher resolution images generally represent finer detail of the flow field with greater fidelity. However, Steinman et al. (19) noted that increasing spatial resolution can result in progressive velocity underestimation as data readout times increase. Additionally, the phantom investigated here was stationary, and although the flow was pulsatile, the vessel walls were rigid. Walls that move, either in a bulk

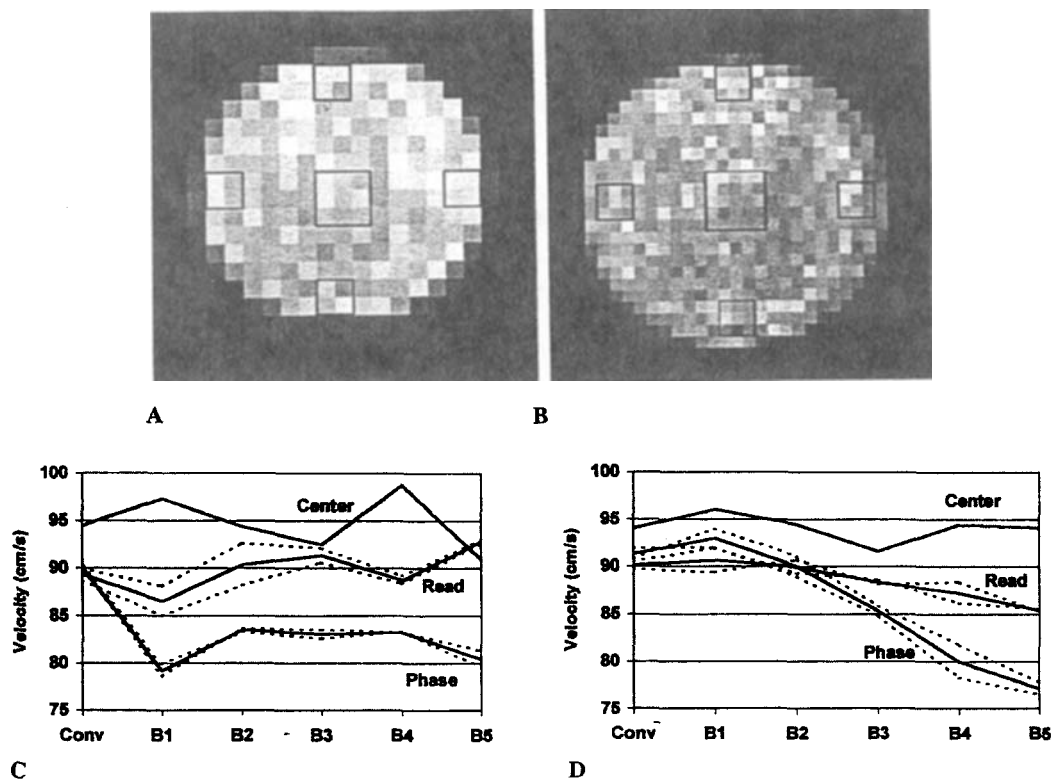


Figure 3. Low- (A) and high-resolution (B) magnitude images for turbo-BRISK, indicating regions chosen for average velocity plots of C and D, respectively. The pair of regions at the 3 and 9 o'clock positions are aligned along the phase-encoding direction. In C and D, the central region is shown as a single solid line and the paired regions are represented by dashed lines, with the mean for each pair plotted as a solid line. Conv, conventional.

Table 4
Results Summary for the In Vivo Study

Volunteer	Stroke Volume (ml)	Adjusted Stroke Volume (ml)	Area (mm ²)	Fourier Coefficients	r	Slope	Intercept	SE
1	102/83	102/100	385/408	3	0.98	0.99	-16.97	15.03
2	94/107	94/73	426/376	4	0.98	0.77	33.99	12.25
3	45/68	45/46	317/345	4	0.99	1.05	19.99	9.36
4	61/83	61/68	277/331	5	0.98	1.12	14.83	22.83
5	54/50	54/55	282/309	5	0.96	1.02	-5.03	13.17

All values relate to flow in the descending aorta. In dual-occupancy fields, the first number is derived from the conventional data and the second number from the turbo-BRISK data. The number of Fourier coefficients with energy above 1% of that of the zeroth coefficient are given, along with the correlation coefficient and regression analysis parameters for conventional vs. turbo-BRISK. The adjusted stroke volume corrects for the offset predicted by regression analysis (see text for details).

fashion or due to compliance, potentially can be blurred by the BRISK acquisition.

In Vivo Results

For the normal volunteer scans, flow parameters for the descending aorta are summarized in Table 4. The integrated velocity over the vessel cross-section is compared for the conventional and turbo-BRISK data sets by regression analysis, revealing an average slope coefficient very close to unity (0.99 ± 0.1), indicating excellent agreement in representation of the flow waveform with respect to both shape and amplitude. However, the average intercept coefficient was significantly different from zero (9 ± 20 ml). A non-zero intercept is indicative of a constant offset between data sets. From these and additional scans (not discussed here) we determined that this offset is not inherent to turbo-BRISK acquisitions but is a processing artifact associated with reconstruction of partial echo data. For comparison purposes, each turbo-BRISK value was adjusted by the offset indicated, reducing the stroke volume difference from 15 ± 28 to $6 \pm 14\%$ ml (Table 4). The adjusted difference in stroke volume is comparable with the variations in the descending aorta cross-sectional area, $6 \pm 11\%$ ml. Fourier analysis of the standardized waveforms showed that on average, 4.2 coefficients had energy above 1% of that of the zeroth coefficient, indicating that the highest frequency information was slightly higher than that of the *in vitro* phantom. Turbo-BRISK was capable of representing these normal waveforms with high fidelity. However, pathologic flow conditions might be expected to result in an increase in the number of significant Fourier coefficients, and further evaluation of turbo-BRISK *in vivo* is warranted.

Images obtained with conventional and breathhold turbo-BRISK are shown in Fig. 4. For the conventional scan, volunteers were instructed to breathe in a light manner, as seen by the nonblurred rendering of the chest wall in Fig. 4A. However, during the approximately 4-min study, flow variations resulted in artifacts comparable in magnitude with true aortic flow as seen in the velocity plot for a static region in Fig. 4A (the image set shown was chosen to highlight the potential impact of respiratory artifacts, which are lower in other series but are nevertheless unpredictable in their manifestation). The corresponding turbo-BRISK image shown in Fig. 4B was acquired at the same resolution during a single breathhold of 20-sec duration. For aortic flow, turbo-BRISK velocity waveforms are similar to those of the conventional scan. Slight flow and motion artifacts were observed in the breathhold turbo-BRISK data series, which were primarily associated with cardiac motion.

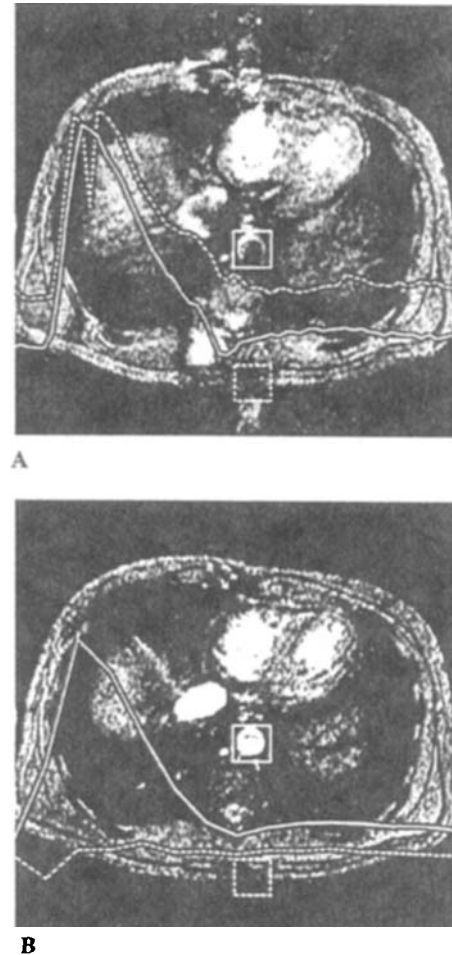


Figure 4. Magnitude images acquired with (A) the conventional scan and (B) the turbo-BRISK scan. Superimposed on the images are the time-resolved mean velocity plots for a 9×8 pixel region in the center of the aorta (solid line) and an 8×8 pixel region of static tissue (dashed line).

CONCLUSIONS

We implemented VEC imaging with BRISK and turbo-BRISK gradient echo acquisitions. Turbo-BRISK with low to moderate turbo factors permits rapid acquisition of high spatial and temporal resolution data sets with accurate representation of velocities *in vitro*. Fine details of the flow field were slightly distorted by the turbo-BRISK sampling strategy. Turbo-BRISK tended to underestimate velocities in the high-velocity gradient region near the vessel wall, which was more pronounced for the lower spatial resolution series and at higher turbo factors. *In vivo* turbo-BRISK scans were performed in a single breathhold, with moderate turbo factors of 3 or 4.

The *in vivo* turbo-BRISK data acquired in one breathhold compared well with the conventional data and accurately represented the flow waveforms (after correction for a constant offset unrelated to BRISK). Turbo-BRISK data acquisitions allowed capturing aortic flow in a single 20-sec breathhold, thereby eliminating significant and potentially unacceptable respiratory artifacts.

REFERENCES

- Nayler GL, Firmin DN and Longmore DB. Blood flow imaging by cine magnetic resonance. *J Comput Assist Tomogr*, 1986; 10:715–722.
- Kilner PJ, Manzara CC, Mohiaddin RH, Pennell DJ, St. John Sutton M, Firmin DN and Longmore DB. Magnetic resonance jet velocity mapping in mitral and aortic valve stenosis. *Circulation*, 1993; 87:1239–1248.
- Mohiaddin RH, Kilner PJ, Rees RSO and Longmore DB. Magnetic resonance volume flow and jet velocity mapping in aortic coarctation. *J Am Coll Cardiol*, 1993; 22: 1515–1521.
- Mohiaddin RH, Underwood SR, Romeira L, Anagnostopoulos CA, Karwatowski SP, Laney R and Sommerville J. Comparison between cine magnetic resonance velocity mapping and first pass radionuclide angiography for quantitating intercardiac shunts. *Am J Cardiol*, 1995; 75: 529–532.
- Eichenberger AC, Schwitter J, McKinnon GC, Debatin JF and von Schulthess GK. Phase-contrast echo-planar MR imaging: real-time quantification of flow and velocity patterns in the thoracic vessels induced by Valsalva's maneuver. *J Magn Reson Imaging*, 1995; 5:648–655.
- Krug B, Kugel H, Harnischmacher U, Heindel W, Schmidt R and Krings F. Phase-contrast pulsatility measurements: preliminary results in normal and arteriosclerotic iliofemoral arteries. *J Magn Reson Imaging*, 1995; 5:201–206.
- Sakuma H, Blake LM, Amidon TM, O'Sullivan M, Szolar DH, Fruber AP, Bernstein MA, Foo TKF and Higgins CB. Coronary flow reserve: noninvasive measurement in humans with breath-hold velocity-encoded cine MR imaging. *Radiology*, 1996; 198:745–750.
- Ligamneni A, Hardy PA, Powell KA, Pelc NJ and White RD. Validation of cine phase-contrast MR imaging for motion analysis. *J Magn Reson Imaging*, 1995; 5:331–338.
- Spritzer CE, Pelc NJ, Lee JN, Evans AJ, Sostman HD and Riederer SJ. Rapid MR imaging of blood flow with a phase-sensitive, limited-flip-angle, gradient recalled pulse sequence: preliminary experience. *Radiology*, 1990; 176:255–262.
- Chatzimavroudis GP, Oshinski JN, Pettigrew RI, Walker PG, Franch RH and Yoganathan AP. Quantification of mitral regurgitation with MR phase velocity mapping using a control volume method. *J Magn Reson Imaging*, 1998; 8:577–582.
- Oshinski JN, Parks WJ, Markou CP, Bergman HL, Larson BE, Ku DN, Mukunda S and Pettigrew RI. Improved measurement of pressure gradients in aortic coarctation by magnetic resonance imaging. *J Am Coll Cardiol*, 1996; 28:1818–1826.
- Walker PG, Oyre S, Pedersen EM, Houlind K, Guenet FSA and Yoganathan AP. A new control volume method for calculating valvular regurgitation. *Circulation*, 1995; 92:579–586.
- Westenberg JJM, Wasser MNJM, van der Geest RJ, Pattynama PMT, de Roos A, Vanderschoot J and Reiber JHC. Variations in blood flow waveforms in stenotic renal arteries by 2D phase-contrast cine MRI. *J Magn Reson Imaging*, 1998; 8:590–597.
- Foo TKF, Bernstein MA, Aisen AM, Hernandez RJ, Collick BD and Bernstein T. Improved ejection fraction and flow velocity estimates with use of view sharing and uniform repetition time excitation with fast cardiac techniques. *Radiology*, 1995; 195:471–478.
- Hofman MBM, Wickline SA and Lorenz CH. Quantification of in-plane motion of the coronary arteries during the cardiac cycle: implications for acquisition window duration for MR flow quantification. *J Magn Reson Imaging*, 1998; 8:568–576.
- Poutanen VP, Kivisaari R, Hakkinen AM, Savolainen S, Hekali P and Nordenstam CGS. Multiphase segmented k-space velocity mapping in pulsatile flow waveforms. *Magn Reson Imaging*, 1998; 16:261–269.
- Keegan J, Firmin D, Gatehouse P and Longmore D. The application of breath hold phase velocity mapping techniques to the measurement of coronary artery blood flow velocity: phantom data and initial *in vivo* results. *Magn Reson Med*, 1994; 31:526–536.
- Davis CP, Liu PF, Hauser M, Gohde SC, von Schulthess GK and Debatin JF. Coronary flow and coronary flow reserve measurements in humans with breath-held magnetic resonance phase contrast velocity mapping. *Magn Reson Med*, 1997; 37:537–544.
- Steinman DA, Ethier CR and Rutt BK. Combined analysis of spatial and velocity displacement artifacts in phase contrast measurements of complex flow. *J Magn Reson Imaging*, 1997; 7:339–346.
- Spielman DM, Pauly JM and Meyer GH. Magnetic resonance fluoroscopy using spirals with variable sampling densities. *Magn Reson Med*, 1995; 34:388–394.
- Doyle M, Walsh EG, Blackwell GG and Pohost GM. Block regional interpolation scheme for k-space (BRISK): a rapid cardiac imaging technique. *Magn Reson Med*, 1995; 33:163–170.
- Liao JR, Pauly JM, Brosnan TJ and Pelc NJ. Reduction of motion artifacts in Cine MRI using variable-density spiral trajectories. *Magn Reson Med*, 1997; 37:569–575.

23. Jhooti P, Gatehouse PD, Mohiaddin RH, Yang GZ and Firmin DN. MR velocity mapping using reduced sampling schemes to shorten the acquisition time. *Proceeding of the Fourth Annual Meeting of the International Society for Magnetic Resonance in Medicine*, New York, NY, April 27 to May 3, 1996, p. 1278.
24. Doyle M, Walsh EG, Foster RE and Pohost GM. Rapid cardiac imaging with turbo BRISK. *Magn Reson Med*, 1997; 37:410-417.
25. Fox JF, Anayiotos AS, Doyle M and Perry GJ. Performance of phase contrast angiography in quantifying valvular regurgitation: an in-vitro model. B10-13, International Mechanical Engineering Congress and Exposition, San Francisco, CA, November 12-17, 1995.
26. Gatehouse PD, Firmin DN, Collins S and Longmore DB. Real time blood flow imaging by spiral scan phase velocity mapping. *Magn Reson Med*, 1994;31:504-512.
27. Underwood SR, Firmin DN, Klipstein RH, Reese RSO and Longmore DB. Magnetic resonance velocity mapping: clinical application of a new technique. *Br Heart J*, 1987; 57:404-412.
28. Frayne R, Steinman DA, Ethier CR and Rutt BK. Accuracy of MR phase contrast velocity measurements for unsteady flow. *J Magn Reson Imaging*, 1995; 4:428-431.